Preparation and Comparison of Supported Gold Nanocatalysts on Anatase, Brookite, Rutile, and P25 Polymorphs of TiO_2 for Catalytic Oxidation of CO

Wenfu Yan,[†] Bei Chen,[†] S. M. Mahurin,[†] V. Schwartz,[†] D. R. Mullins,[†] Andrew R. Lupini,[‡] S. J. Pennycook,[‡] Sheng Dai,*[,†] and S. H. Overbury*[,†]

Chemical Sciences Division and Condensed Matter Physics Division, Oak Ridge National Laboratory, Oak Ridge, Tennessee, 37831-6201

Received: December 28, 2004; In Final Form: March 4, 2005

Nanosized anatase (≤10 nm), rutile (≤10 nm), and brookite (~70 nm) titania particles have been successfully synthesized via sonication and hydrothermal methods. Gold was deposited with high dispersion onto the surfaces of anatase, rutile, brookite, and commercial titania (P25) supports through a deposition−precipitation (D−P) process. All catalysts were exposed to an identical sequence of treatment and measurements of catalytic CO oxidation activity. The as-synthesized catalysts have high activity with concomitant Au reduction upon exposure to the reactant stream. Mild reduction at 423 K produces comparably high activity catalysts for every support. Deactivation of the four catalysts was observed following a sequence of treatments at temperatures up to 573 K. The brookite-supported gold catalyst sustains the highest catalytic activity after all treatments. XRD and TEM results indicate that the gold particles supported on brookite are smaller than those on the other supports following the reaction and pretreatment sequences.

1. Introduction

Until about 10 years ago, gold was generally regarded to be poorly active as a catalyst. However, the early studies of Bond et al.,[1] Ozin et al.,[2,3] and Parravano et al.[4,5] indicated that gold is chemically active when it is dispersed as nanoparticles. In the late 1980s and the early 1990s, Haruta et al. found that the gold particles deposited on selected metal oxides exhibit surprisingly high catalytic activity for CO oxidation even at 200 K.[6,7] Now, extensive literature describes the CO oxidation ability of gold nanoparticles supported on metal oxides such as TiO_2,[8−19] Fe_2O_3,[6,20] Co_3O_4,[6] NiO,[6] SiO_2,[21] Al_2O_3,[22,23] and ZrO_2[24,25] and alkaline earth metal hydroxides such as $Be(OH)_2$ and $Mg(OH)_2$,[26,27] which have been well reviewed.[28−36] In general, a wide variation in activity of the Au catalysts has been observed between different supports.

Much of the variability in Au catalysts supported on different oxides derives from variation in the properties of the oxides, for example, the effect of isoelectronic point on the deposition of Au or the role of the oxide reducibility as it affects the transfer of oxygen between the support and the Au nanoparticles. To understand more deeply the mechanism of catalysis of the gold nanoparticles deposited on metal oxides, it is of interest to study the effects of variability of support structure for a single type of oxide. TiO_2 is a good candidate because it exists in three main different allotropic forms: anatase, brookite, and rutile. Most of the previous studies on the Au−TiO_2 system are focused on the deposition of gold on commercial titania Degussa P25, a TiO_2(110) surface,[37,38] a TiO_2(001) surface,[16] or titania aerogels.[39] Studies of the deposition of gold nanoparticles on the pure titania phase of anatase,[20] rutile, or brookite[40] are rare. Previously published work has demonstrated that the photocatalytic efficiency of titania depends on its crystalline form. This variability has been attributed to differences in the rates of recombination, adsorptive affinity, or band gap between the rutile and anatase phases of titania.[41−43] Mo et al. found computationally that anatase has a larger band gap than rutile, although they both have similar ground-state properties.[44] It has been pointed out that the Fermi level in anatase is higher than that of rutile by about 0.1 eV.[45] In titania containing mixed phases of rutile and anatase, such as Degussa P25, enhanced activity for photocatalytic oxidation may also depend on crystallite morphology and interfacial contact.[43] It is therefore of interest to understand how differences in the structure of a titania support may affect other oxidative catalytic processes in Au catalysts. It has been shown that the selectivity in propylene epoxidation is improved by using anatase compared to rutile for catalysts prepared by deposition−precipitation (D−P) of Au.[46] Higher activity for CO oxidation is observed for anatase compared to rutile when Au is deposited using a rather unconventional ion-cluster beam deposition approach.[47] The deactivation of Au catalyst particles supported on TiO_2 for CO oxidation has been observed to be dependent upon the support structure.[40] The contacts at the Au−TiO_2 interfaces are also believed to play an important role in CO oxidation.[48]

In pure undoped TiO_2, both metastable phases convert to rutile upon heating the material at temperatures above 700 °C.[49] In all three phases, the coordination of Ti is 6-fold with oxygen anions forming a distorted octahedron, and the oxygen atom is shared by three adjacent Ti atoms. However, distortions of the octahedra in these three phases lead to crystallographic differences and result in the different arrangement of the Ti−O and Ti−OH bonds on the surface of their particles. The titanium ions in both rutile and anatase are located in tetragonal sites, in which two axial Ti−O bonds are longer than four equatorial Ti−O bonds. The distortion of the [TiO_6] unit is greater in anatase than in rutile. Two edges of the [TiO_6] unit are shared in rutile, whereas four edges are shared in anatase. The structural

* Corresponding authors. E-mail: dais@ornl.gov. E-mail: overburysh@ornl.gov. Phone: 865-574-5040. Fax: 865-576-5235.
[†] Chemical Sciences Division.
[‡] Condensed Matter Physics Division.

10.1021/jp044091o CCC: $30.25 © 2005 American Chemical Society
Published on Web 05/06/2005

distortion of the [TiO_6] unit in brookite is the greatest among the three allotropic phases, having six different Ti−O bond lengths.[50] The structures of the most stable surfaces of TiO_2 have been examined for rutile and antase.[51] Both the (101) surface of anatase and the (110) surface of rutile exhibit 2-fold coordinate oxygen anions and 5-fold Ti cations, but the oxygen anions are more widely spaced on the anatase surface. The different spacing and symmetry of these Ti−O and −OH bonds on the surface of the particles of anatase, brookite, and rutile might affect the deposition of the gold hydroxyl precursor on the surface of the titania particles during the D−P process. The systematic study of the reaction on anatase-, brookite-, rutile-, and P25-supported gold catalysts might allow new insight into the catalytic mechanism of the gold nanoparticles deposited on the metal oxides.

In the following, we present the results of studies of catalysts prepared and tested by identical procedures in Au catalysts supported on all three of the pure TiO_2 polymorphs as well as on P25. We find that when other factors are kept constant, the catalytic activity is not much affected by the variation of the titania structure. However, the stability of the Au nanoparticles is dependent upon the support structure. In addition, many previous studies on the preparation of the TiO_2-supported gold catalysts involved the calcinations at elevated temperature between 473 and 673 K to control the particle size of the gold on the metal oxide supports. Our results indicate that the as-synthesized titania-supported gold catalyst and catalysts reduced at 423 K show high activity. High resolution transmission electron microscopy (HRTEM) analyses on the most active samples show predominantly 0.5−2 nm sized gold particles on the surface of the titania surface.

2. Experimental Section

2.1. Sonication Synthesis of Anatase and Rutile. In a typical synthesis, 100 mL of deionized water was sonicated by employing a direct immersion titanium horn (Sonics and Materials, VCX-750, 20 kHz, starting power 100 W) followed by the injection of 10 mL of the Ti precursor into the sonication cell (glass beaker). The structure of the resulting oxide depends on the type of precursor, and using tetraisopropyltitanate (Aldrich) leads to anatase while using titanium tetrachloride (Aldrich) leads to rutile.[52] The mixture was further sonicated continuously for 1 h, and the sonication was conducted without cooling. The white precipitates were separated by centrifugation at 8000 rpm (about 8200*g*) and washed three times with deionized water and once with ethanol. After each centrifugation, the clear liquid was decanted and the solid product was redispersed into solvent for the next washing cycle. Finally, the product was dried in a desiccator overnight and was ground into a fine powder before the deposition of the gold precursor on its surface.

2.2. Hydrothermal Synthesis of Brookite.[53] Typically, NaOH solution (2 M) was added to 5 mL of titanium tetrachloride with stirring to adjust the pH value of the solution to 10, producing a basic colloidal solution. The obtained solution was transferred into an autoclave and heated at 200 °C for 24 h. The white precipitates were separated by centrifugation and washed three times with deionized water and once with ethanol, as described in section 2.1. The product was dried at 70 °C in air overnight. The product was ground to a fine powder before the deposition of the gold precursor on its surface.

2.3. Deposition−Precipitation (D−P) of the Gold Precursor on Anatase, Brookite, Rutile, and Commercial P25. First, weighed amounts of hydrogen tetrachloroaurate (III) trihydrate ($HAuCl_4 \cdot 3H_2O$, 99.9+%, Aldrich) were dissolved into 50 mL of deionized water. The pH value of the resulting solution was adjusted to between 9.0−10.0 with vigorous stirring using a solution of 1.0 M KOH at room temperature to displace Cl^- with hydroxyl on the Au precursor.[54] After pH adjustment, the solution was heated in a 60 °C water bath followed by the addition of 1.0 g of TiO_2 powder. The resulting mixture was continually stirred for 2 h to permit the Au precursor to react with and displace surface hydroxyls. Finally, the precipitates were separated by centrifugation and washed three times with deionized water and once with ethanol to remove Cl^-. The product was dried at a 50 °C temperature in air overnight to obtain the "as-synthesized" catalyst. To avoid growth of Au particles and other changes in the catalysts, no calcinations or reductions were performed on the catalysts until they were put into the catalytic reactor.

TABLE 1: Loading and Surface Area of As-Synthesized Catalysts

TiO2 support type	synthesis loading	ICP loading (%)	XANES loading (%)	surface area (m^2/g)	Au areal density in units of (111) monolayers[a]
anatase	13	13	10.0[b]	225	0.12
anatase	6	5.2	n/a	225	0.051
anatase	3	2.8	n/a	225	0.027
brookite	13	3.3	2.7[b]	106	0.069
rutile	13	14	11.9[b]	77	0.39
rutile	6	2.9	n/a	77	0.083
P25	13	5.7	4.1[b]	47	0.27
P25	13	7.2	8.	47	0.34
P25	6.5	4.5	5	47	0.21

[a] Based on ICP loadings, in units of Au(111) monolayer or 13.9×10^{18} Au/m^2. [b] XANES loading normalized to neutron activation analysis loading measured for anatase.

The amount of Au that would be expected if all Au adsorbed on the titania support was calculated from the synthesis parameters and is reported in Table 1 as the "synthesis" loading. The actual Au loadings of the samples were determined using inductively coupled plasma-atomic absorption (ICP-AA). A set of dissolved $HAuCl_4$ solutions were obtained (Alfa-Aesar) and used as standards for ICP-AA analysis. The supported Au catalysts were digested in $HCl-HNO_3$ intended to dissolve the Au and the TiO_2 support. The dissolved samples were run along with the standards. Since the measurements were performed on as-synthesized samples which contain 2−8% water (according to thermogravimetric analysis (TGA) data), then the reported Au loadings are low by this amount compared to the dry loadings. The step edge measured by X-ray absorption near-edge spectroscopy (XANES) was also used as a semiquantitative measure of Au concentration. The Au−anatase sample with the highest synthesis loading was checked by neutron activation analysis, which was used to normalize the edge jump for four of the XANES measurements. The results from these three methods are provided in Table 1. There is qualitative agreement between the XANES and ICP measurements.

2.4. Measurements of Catalytic Performance for CO Oxidation. The CO oxidation reaction was carried out in a plug flow microreactor (AMI 200 Altamira Instruments). Typically 50 mg of Au−TiO_2 catalyst was packed into a 4 mm i.d. quartz U-tube, supported by quartz wool. Sample treatments were carried out on the same instrument using 8% O_2−He for oxidations, 12% H_2−Ar for reductions, or Ar for thermal treatment. For each treatment, gas flow was initiated near room temperature and then the temperature was ramped at 10 °C/min to the target and held for 30 min, and then cooled to reaction temperature in the gas. Each pretreatment was followed by

SCHEME 1

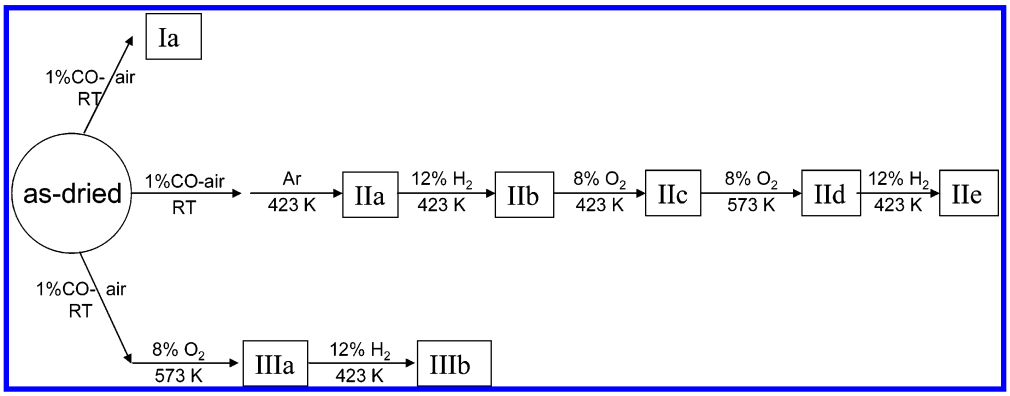

activity measurements made as follows. A gas stream of 1% CO balanced with dry air (<4 ppm water) was flowed at ambient pressure through the catalyst at a rate that was adjusted from sample to sample to maintain a constant space velocity of 44 000 mL/(h·g of catalyst) or about 37 cm^3/min. Gas exiting the reactor was analyzed by a Buck Scientific 910 gas chromatograph equipped with a dual molecular sieve/porous polymer column (Alltech CTR1) and using a thermal conductivity detector. Typically, the sample was cooled to low temperature and the exiting gas was analyzed at regular intervals as the sample was slowly warmed. The reaction temperature was varied using an oven or by immersing the U-tube in a dewar of ice water or of cooled acetone which slowly warmed (typically 0.1−0.2 °C/min) throughout approximately 10 h. The resulting curve of conversion versus temperature was used to assess the activity after each treatment. An identical treatment protocol was followed for each sample. Four different aliquots of each catalyst were run, each treated according to the following reaction and treatment sequences, illustrated in Scheme 1:

(I) The as-synthesized sample was exposed to a reaction mixture (1% CO−air) for about 1 h at room temperature. It was then cooled to low temperature, and activity was measured with increasing temperature.

(II) The as-synthesized sample was exposed to the reaction mixture for approximately 1 h at room temperature, and then, a sequence of treatment steps were carried out, with each step followed by measuring a light-off curve. The sequence consisted of the following five steps: (a) heating in Ar at 423 K for 30 min, (b) reduction at 423 K for 30 min, (c) oxidation at 423 K for 30 min, (d) oxidation at 573 K for 30 min, and (e) reduction at 423 K for 30 min. After each of these treatment steps, the sample was cooled in the treatment gas and then a light-off curve was measured, implying long exposure to the reaction mixture at temperatures below 373 K.

(III) The as-synthesized sample was exposed to the reaction mixture for approximately 1 h at room temperature and then a sequence of treatments carried out, each step followed by measuring a light-off curve. The sequence consisted of the following two steps: (a) oxidation at 573 K for 30 min and (b) reduction at 423 K for 30 min. After both treatment steps, the sample was cooled in the treatment gas and then a light-off curve was measured, implying long exposure to the reaction mixture at temperatures below 373 K.

(IV) The as-synthesized sample was oxidized at 773 K for 30 min and then cooled in the treatment gas prior to measurement of the light-off curve.

2.5. Characterization Methods. Powder X-ray diffraction (XRD) data were collected via a Siemens D5005 diffractometer with Cu Kα radiation ($\lambda = 1.5418$ Å). Microscopy was carried out on two different microscopes. Routine TEM and Z-contrast microscopy was carried out using an HITACH HD-2000 scanning transmission electron microscope operated at 200 kV. A VG 603 aberration corrected Z-contrast microscope capable of magnifications up to 5×10^7 was employed for the high resolution microscopy. Nitrogen gas adsorption measurements (Micromeritics Gemini) were used to measure the surface area and porosity of the titania supports.

X-ray absorption near-edge spectroscopy (XANES) was performed at the NSLS at beamline X-18b. Samples were diluted with BN and pressed into pellets which were placed in a quartz reactor tube. An oven permitted treating the samples at elevated temperatures in flowing hydrogen (4% H_2−He), the reaction mixture (1% CO−air), or Ar. XANES spectra were measured in fluorescence mode following various pretreatments and were used to determine the Au loading and the oxidation state of the Au catalysts. XANES results are described in more detail elsewhere.[55]

3. Results

3.1. Characterization of the Catalysts. *Au on Anatase.* The powder XRD patterns shown in Figure 1 show that the TiO_2 synthesized by sonication is well described as the anatase phase, although it contains a small amount of brookite impurity. The scanning electron microscopy (SEM) micrograph in Figure 2 shows a very fine particle size of the sonicated anatase, composed of approximately 5−10 nm particles which are aggregated together to form bigger assemblies. It is believed that the interparticle mesopores are responsible for the hysteresis loop observed in the N_2 adsorption isotherm (Supporting Information Figure s1). These interparticle mesopores are an important contribution to the measured high Brunauer−Emmett−Teller (BET) surface area 225 m^2/g.

After the D−P of the gold precursor on the surface of the anatase support, the XRD pattern is unchanged; in particular, no metallic gold peaks are observed in XRD (Figure 1). Since the Au loading is high, the lack of additional peaks due to the Au D−P indicates that the gold is highly dispersed into particles that are too small to generate observable XRD peaks. XANES analysis of the catalyst in this as-synthesized state indicates that a substantial amount of the Au is in a cationic state. A Z-contrast micrograph of the as-synthesized anatase-supported gold catalyst (Figure 3, top) shows a broad distribution of gold particles resulting from the D−P including aggregates, as large as 20−50 nm, but their concentration must be too low to give detectable XRD peaks. Higher resolution Z-scanning transmission electron microscopy (Z-STEM) analyses reveal many raftlike, small particles in the size range 0.5−2.0 nm are present in the as-synthesized catalyst (Figure 3, bottom). On the basis

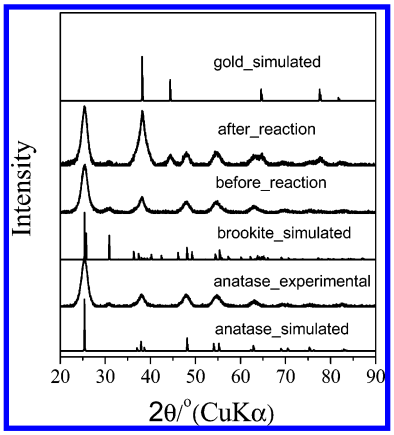

Figure 1. Simulated XRD patterns for anatase, brookite, and gold compared with experimental XRD for anatase and anatase-supported gold catalyst (13 wt % Au). The Au loaded catalyst is shown both in the as-synthesized state and after exposure in the reactor to treatment sequence II.

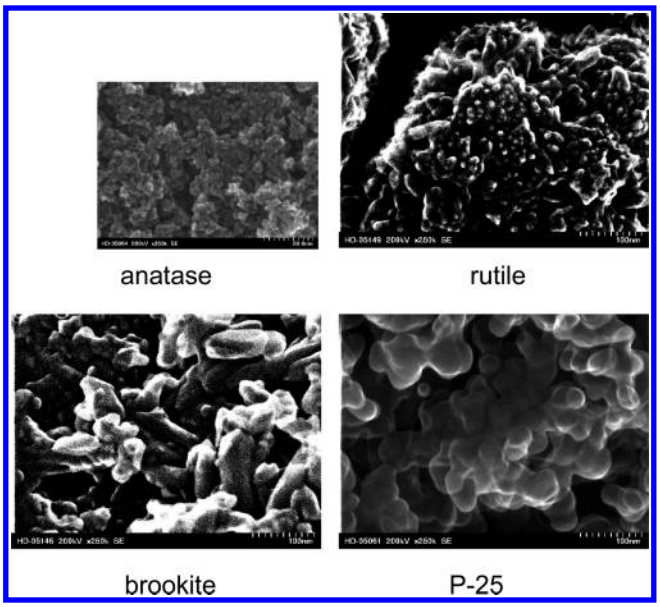

Figure 2. SEM micrographs of the different titania polymorphs shown (at the same magnification) before deposition of Au.

of the XANES results, it is concluded that these small rafts are primarily Au oxide or Au oxyhydroxide.

Samples were also examined after removal from the catalytic reactor. In one case, a catalyst was removed from the reactor at the end of sequence II, including oxidation to 573 K. XRD showed obvious gold peaks (Figure 1), indicating an increase in the concentration of metallic gold particles large enough to generate detectable XRD peaks (larger than about 5 nm). In another case, the catalysts were reduced at 573 K in H_2 and subsequently oxidized at 773 K, followed by another reduction at 423 K, a sequence which substantially deactivated the sample. Microscopy indicated complete loss of the raftlike small particles and the appearance of large faceted Au nanoparticles with sizes 10 times larger, that is, in the range 5−20 nm (not shown).

Au on Rutile. In contrast to anatase obtained using the sonication method, rutile prepared by the same methodology did not contain any XRD detectable impurity (Figure 4). The SEM micrograph of nanocrystalline rutile (Figure 2) exhibits facets which appear to be larger than those of the anatase. A larger particle size for rutile is in agreement with the observed narrower XRD peaks (Figure 4 vs Figure 1) and with the results of Huang et al.[52] Larger particles partly explain the smaller

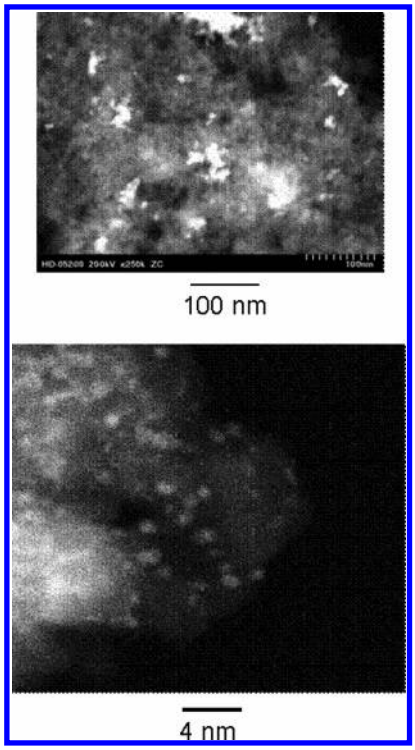

Figure 3. Images by conventional (250 000 magnification, top) and high resolution (2×10^7 magnification, bottom) Z-contrast STEM micrographs of as-synthesized gold−anatase catalyst (13 wt % Au).

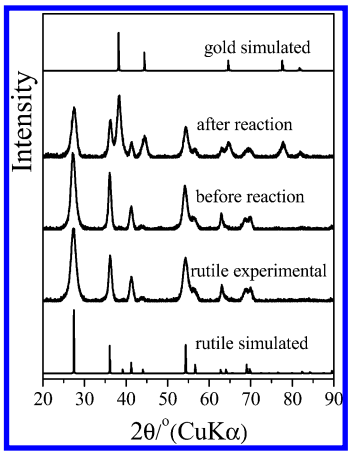

Figure 4. Simulated XRD patterns for rutile and gold compared with experimental XRD for rutile and rutile-supported gold catalyst (14 wt % Au). The Au loaded catalyst is shown both in the as-synthesized state (before reaction) and after exposure in the reactor to treatment sequence II (after reaction).

measured BET surface area, 77.5 m^2/g, observed for rutile. In addition, a slightly less pronounced hysteresis loop is observed for rutile than for anatase, suggesting a smaller surface area associated with mesoporosity in rutile (Supporting Information Figure s2, N_2 adsorption isotherm of sonicated rutile).

After Au D−P, the rutile-supported gold catalyst did not give detectable gold XRD peaks, despite a high Au loading (Figure 4), similar to the result for the anatase-supported gold catalyst. As with the anatase-supported sample, XANES indicates again that the Au is present primarily in an oxidized phase. No clear Au particles were observed on the as-synthesized Au catalyst by conventional TEM, although the Z-contrast indicated broad, diffuse regions containing Au (not shown). As with the anatase, after it was subjected to the catalytic reaction conditions (sequence II, see below), this catalyst gives obvious gold XRD

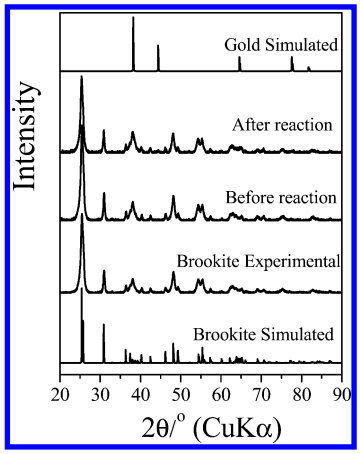

Figure 5. Simulated XRD patterns for brookite and gold compared with experimental XRD for brookite and brookite-supported gold catalyst (3.3 wt % Au). The Au loaded catalyst is shown both in the as-synthesized state (before reaction) and after exposure in the reactor to treatment sequence II (after reaction).

peaks, indicating the reduction and aggregation of Au into nanoparticles that are at least 5 nm in average diameter in agreement with STEM observations.

Au on Brookite. Synthesis of TiO_2 under the hydrothermal process gave single phase brookite, as indicated by the comparison of the simulated and experimental powder XRD patterns shown in Figure 5. The nanocrystallites of brookite, obtained through the hydrothermal process, are bigger than those of rutile or anatase, and many are needlelike, in agreement with the sharper XRD features. The SEM micrograph shows that the characteristic particle size of the brookite is on the order of 70 nm (Figure 2). Surprisingly, the measured BET surface area 106 m^2/g (Supporting Information Figure s3, N_2 adsorption isotherm of hydrothermal synthesized brookite) is larger than that of finer grained rutile (77 m^2/g) although smaller than that of anatase (225 m^2/g). The more pronounced hysteresis loop in nitrogen adsorption indicates that interparticle mesopores exist in the brookite and are responsible for the relatively high surface area.

As-synthesized brookite-supported gold catalyst did not give detectable gold XRD peaks (Figure 5). In contrast with anatase- and rutile-supported gold catalysts, after exposure to catalytic reaction conditions (following sequence II), the brookite-supported gold catalyst still did not exhibit obvious gold XRD peaks (note the absence of a peak near 45°). Although the Au loading is low, the Au peaks should still be visible if the mean Au particle size was as big as that observed on rutile. The results suggest small Au particle sizes are stable to the reaction conditions in sequence II. Z-contrast microscopy results were obtained on this sample in three different states: (1) the as-synthesized state, (2) after reduction at 423 K, and (3) following calcination of the sample at 573 K. Micrographs in each of these states are shown in Figure 6. As with the anatase, Au is visible in the as-synthesized state as very small, apparently thin rafts with sizes of 0.5−2 nm (Figure 6a). Little is changed following mild treatment at 423 K (Figure 6b). The lattice fringes of the needlelike TiO_2 crystallite are readily visible also in both micrographs. After the calcination at 573 K, these small rafts were not observed, and Au particles were few or absent in several micrographs obtained at the highest magnification. Figure 6c shows a micrograph which exhibits a single Au particle which is 2−3 nm in size and exhibits fringes, suggesting a faceted 3-D particle. At lower magnification, many particles

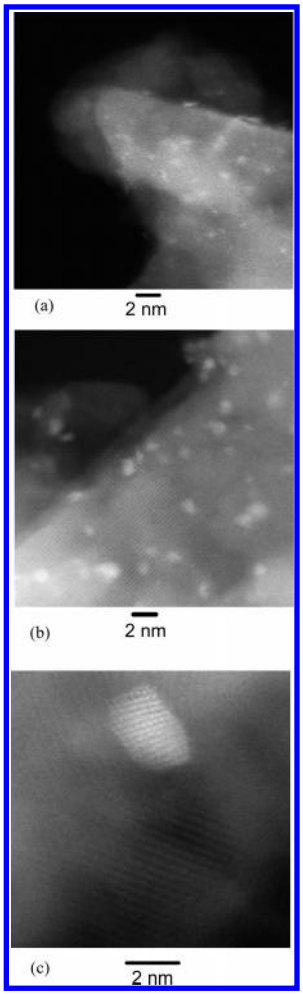

Figure 6. HRTEM micrograph of Au on brookite−gold catalysts recorded (a) in the as-synthesized state, (b) following mild reduction at 423 K, and (c) following calcination at 573 K. The micrographs in parts a and b were obtained at a 2×10^7 magnification, and that in part c was obtained at a 5×10^7 magnification.

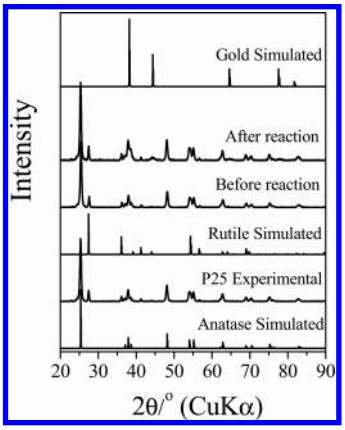

Figure 7. Simulated XRD patterns for anatase, rutile, and gold compared with experimental XRD for P25 and P25-supported gold catalyst (5.7 wt % Au). The Au loaded catalyst is shown both in the as-synthesized state (before reaction) and after exposure in the reactor to treatment sequence II (after reaction).

distributed in the range 1−10 nm are visible, and still lower magnification reveals also many particles in the range 30−70 nm.

Au on Commercial P25. Degussa P25 is a commercially available titania, which contains 70 wt % anatase and 30 wt % rutile. Our XRD results confirm this mixture of phases (Figure

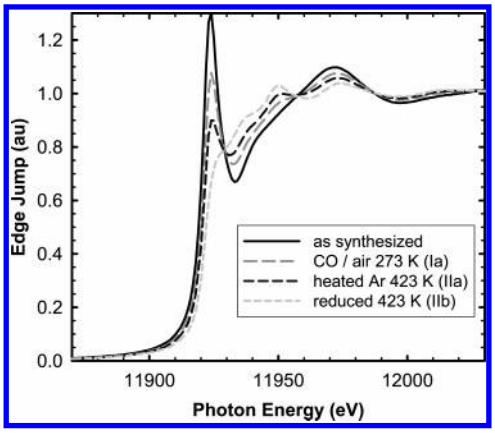

Figure 8. Au XANES spectra of the 14 wt % Au−rutile sample recorded (a) in the as-synthesized state, (b) after exposing it to the reaction mixture of 1% CO−air for 50 min, (c) after heating it to 473 K in Ar for 30 min, and (d) after reducing it for 30 min in 4% H_2−He. The spectra were collected using a fluorescence detector.

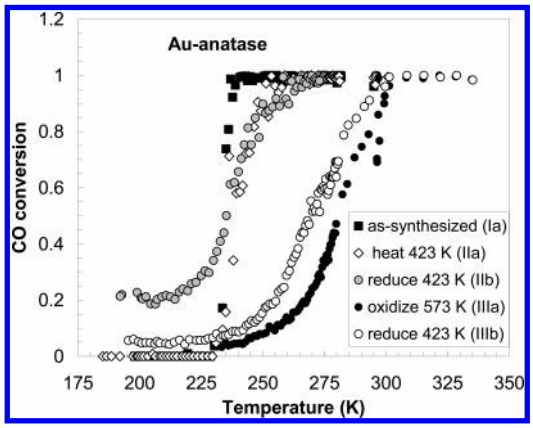

Figure 9. CO oxidation activity over 13 wt % Au−anatase shown as CO conversion vs temperature (light-off curves) after various pretreatment steps.

7). The mean TiO_2 particle size is about 20−30 nm, which is in agreement with the SEM analyses (Figure 2). The measured BET surface area 47 m^2/g is in agreement with the reported value (Supporting Information Figure s4, N_2 adsorption isotherm of P25). Similar to anatase-, rutile-, and brookite-supported gold catalysts, P25-supported gold catalyst did not give any gold peaks before catalyzing the oxidation reaction of CO to CO_2 (Figure 7), although Au is faintly visible after exposure to reaction sequence II. ICP analysis gives a gold concentration of 5.7 wt %.

3.2. Reduction Studies by XANES. XANES was used to extract information about the oxidation state of the Au during the pretreatment steps used in each of the sequences. Typical XANES spectra are shown for the 14 wt % Au−rutile surface in Figure 8 and are further described elsewhere.[55] The pre-edge of the Au L_{III} absorption edges exhibits a sharp peak for the as-synthesized state, indicating that it is highly oxidized, probably mostly in the Au^{3+} state.[55] This peak is slowly diminished by exposure to the reaction mixture of 1% CO−air at room temperature (Figure 8), a condition which mimics that during step Ia. This result demonstrates that reaction conditions at room temperature bring about partial reduction of the Au, even though an excess of oxygen is present. Heating in Ar causes an additional decrease of the peak, indicating that some autoreduction is possible due to heating. Finally, reduction at 423 K, the pretreatment of step IIb, causes a complete loss of the peak and leaves a spectrum which, except for slightly less

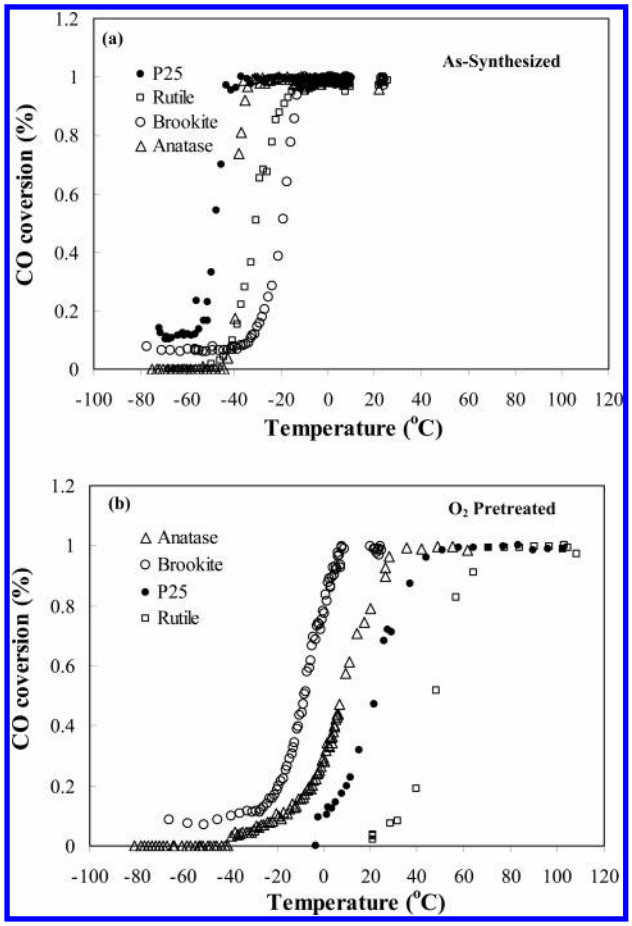

Figure 10. CO oxidation activity over Au−TiO_2 catalysts with different supports: (a) from the as-synthesized sample (step Ia); (b) following treatment in 8% O_2−He pretreated at 573 K for 30 min (step IIIa).

pronounced oscillations, closely matches that of a Au foil (not shown). Additional treatments in hydrogen and in oxygen were performed up to 573 K, and subsequent spectra were run in the CO−air mixture. These treatments did not further alter the general shape of the spectrum or bring about any growth of the peak at the Au edge. Therefore, no reoxidation occurs as a result of these treatments or of exposure to reaction conditions.

3.3. Catalytic Measurements. A typical set of light-off curves are shown in Figure 9 for the 13 wt % Au−anatase sample after various steps of the reaction sequences. For this sample, the as-synthesized catalyst showed 100% conversion at room temperature (298 K) when placed in the reactor. Measurable conversion ceased when cooled to 200 K but resumed as the temperature was increased to above about 235 K (Ia). The curves in Figure 9 show similar behavior after each pretreatment, but the temperature range at which conversion increases changes after each treatment. Similar families of light-offs were obtained for all of the supports.

Light-off curves for the different supports are compared in Figure 10a for the as-synthesized samples and in Figure 10b for the samples which have been oxidized to 573 K in sequence III. Since most light-off curves have a fairly similar shape, it is helpful to describe the activity by the temperature at which the conversion equals 50%, T_{50}. Table 2 summarizes the T_{50} values of all samples after various pretreatments. Values of T_{50} are provided in Figure 11 for three of the catalysts after the various pretreatments. As another indication of the activity, calculated specific reaction rates are given in Table 3, extracted from the light-off curves and normalized to the total ICP Au loadings.

TABLE 2: $T_{50\%}$ of Au−TiO_2 Catalysts for the CO Oxidation Reaction

		T_{50} (K)								
step	pretreatment	13% Au−anatase	5.2% Au−anatase	2.8% Au−anatase	3.3% Au−brookite	14% Au−rutile	2.9% Au−rutile	5.7% Au−P25	7.2% Au−P25	4.5% Au−P25
Ia	as-synthesized	235	252	318	254	242	n/a	225		
IIa	Ar, 423 K	240	264	334	257	260	423	215		
IIb	12% H_2 423K	235	247	293	235	238	>425	248	236[a]	243[a]
IIc	8% O_2 423 K	245	258	296	258	275	>425	316		
IId	8% O_2 573 K	283	253	281	238	327	>425	337	258[a]	246[a]
IIe	12% H_2 423 K	277	264	277	267	321	>425	346		
IIIa	8% O_2 573 K	280	286	279	263	321		294		
IIIb	12% H_2 423 K	269	273	273	258	311		299		
IV	8% O_2 773 K			363	304				411	376

[a] Skipped steps IIa and IIc.

TABLE 3: Comparison of Specific Reaction Rates (mol of CO/mol of total Au·s) at 235 K for Au−TiO_2 Catalysts after Various Treatments[a]

		rate (s^{-1}) × 10^{+3} at 235 K			
support	Au wt % loading (ICP)	reduced 423 K (step IIb)	oxidized 573 K step IId)	oxidized 573 K (step IIIa)	reference
anatase	13	4.0	0.75	0.28	present
anatase	5.2	2.2	3.2	0.35[b]	present
anatase	2.8[c]	1.6	1.6	1.3	present
brookite	3.3	16	15	3	present
rutile	14	1.8	0.0016[b]	0.00003[b]	present
rutile	2.9	0.005[b]	0.006[b]	n/a	present
P25	5.7	7.0	0.07[b]	0.07[b]	present
P25	7.2	4.4	1.4	n/a	present
P25	4.5	8	3.7	n/a	present
World Gold Council (P25)	1.5			23	present
P25[d]	1.8			7.7	ref 12
P25[d]	0.7			2.6	ref 12
P25 calcine 473 K	1			13	ref 19
P25 calcine 573 K	1			22	ref 19

[a] Space velocity = 44 000 (mL/h g of cat.), CO = 1%, O_2 = 20% N_2 balance. [b] Extrapolated. [c] Loading assumed from synthesis stoichiometry. [d] Calcined 673 K, reduced 1% H_2 at 723 K.

Although O_2 chemisorption methods are available,[56] we did not measure Au surface areas, so rates based on surface Au are not reported. These rates are compared with literature values. In addition, a reference catalyst obtained from World Gold Council (WGC) was also run using the same conditions as the other catalysts. Since this catalyst was already calcined by the manufacturer, this catalyst was only pretreated by oxidizing at 573 or 773 K.

All as-synthesized catalysts were light tan or creamy brown in color. When a fresh sample was put into the reactor, a darkening along the upstream edge occurred immediately upon introducing the reaction mixture (1% CO−air), even at room temperature. The darkening was associated with the reduction of Au particles by CO, demonstrated by the XANES measurements described above. Color change was partial or slow at room temperature because the reduced portion of the sample is catalytically active, thereby removing the reductant CO before it could penetrate into the center of the catalyst bed. Exposure in the reaction mixture at room temperature for an hour was not always sufficient to completely reduce the sample, although the process of measuring a full CO light-off curve at temperatures at or below room temperature may fully reduce the as-synthesized sample, changing the entire bed to a dark bluish or black color. Therefore, the extent of reduction may vary throughout the light-off curves obtained after step Ia. However, treatment in H_2 at 423 K (step IIc) or O_2 at 423 K (step IIIa) caused complete reduction, as indicated by color change and proven by XANES.

To better understand the processes occurring under thermal treatment, some of the as-synthesized catalysts were analyzed by temperature-programmed desorption (TPD). Figure 12 shows a TPD curve obtained from the 12.5% Au−anatase sample. In this measurement, the as-dried catalyst was heated from room temperature at 15 K/min under He at a constant flow rate and the desorption products were analyzed by an in-line sample mass spectrometer. The results show that the major product desorbed is water which mostly desorbs below 573 K. Water is attributed both to desorption from the support and dehydrolysis of the Au hydroxide. Au oxide, remaining after the dehydrolysis, decomposes by 573 K to yield an O_2 peak. XANES indicates that the Au oxide is reduced at lower temperatures under hydrogen. A small amount of carbonate also desorbs near 473 and 600 K.

4. Discussion

There have been several studies on the activity of Au catalysts prepared on titania supports, but most studies use Degussa P25 as a support. The present work is apparently the first time that Au catalysts have been prepared and examined on all three polymorphs of titania. The primary goal was to determine if there is an effect of the titania support crystallographic structure on the activity and stability of the resulting Au catalysts. Starting with the four different TiO_2 supports, considerable care was taken to ensure identical Au deposition methods, sample pretreatments, and catalytic testing conditions for each of the catalysts. A sequence of pretreatments was undertaken to study how each is affected by changes in the catalyst makeup during the pretreatments. Observed differences in catalytic activity or stability may then result from differences in how each support

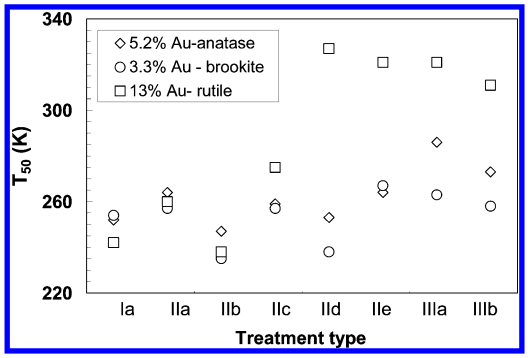

Figure 11. Summary of the light-off temperatures, T_{50}, given for three of the catalysts after the treatments of sequences I, II, and III.

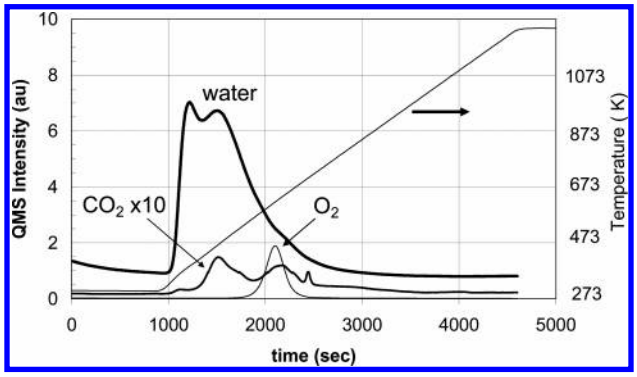

Figure 12. TPD spectra for the 13% Au−anatase sample in He and a heating rate of 15 K/min.

affects the uptake, reducibility, growth, or dispersion of the gold particle growth during thermal treatments.

It is seen that the as-synthesized catalysts are very active. Every catalyst except one exhibited 100% CO conversion at room temperature as soon as reactants were introduced and yielded T_{50} values in a range of about 230−250 K during subsequent light-off (step Ia). These values of T_{50} are as low as those for any other pretreatments. Therefore, it is not necessary to calcine or reduce the catalysts at elevated temperatures to activate it, in agreement with recent results of Moreau et al.[57] Either an active form of Au is present in all the as-synthesized catalyst or Au is immediately converted to an active form by exposure to the reaction mixture at room temperature.

XANES indicates that the Au is present in an oxidized form, presumably as hydroxide, in the as-synthesized catalysts (Figure 8). Both XANES and the sample color changes indicate that the hydroxide is reduced by the CO in the reaction mixture and so CO_2 production results from reduction of Au hydroxide. At the CO flow rates used in the catalytic measurements, sufficient CO is available to achieve complete stoichiometric reduction of all the Au in a few minutes if no CO is lost to competing catalytic conversion. Therefore, CO conversion beyond the first few minutes must be partly associated with *catalytic* conversion of CO. In the as-synthesized catalysts, the Au changes gradually from the oxidized to reduced oxidation state during the process of collecting the light-off curve in step I. Therefore, the measured conversion is ambiguous because it may result from both processes.

Pretreating the catalysts at 423 K in Ar (step IIa) has little effect on the activity as compared to the as-synthesized catalysts (Ia). In most cases, the T_{50} value increases only slightly (Table 2). XANES indicates partial reduction of the Au occurs during heating. Since there is no reductant gas, the autoreduction process is probably dehydrolysis of the Au hydroxide and decomposition of the resulting Au oxide, as suggested by the TPD in Figure 12. Once in the reactant mixture, further reduction may occur analogously to the as-synthesized catalysts. TPD indicates that much of the water on the catalyst desorbs by heating to 423 K, and some sintering of the reduced Au particles might be expected. Previous work has indicated that Au activity is enhanced by water adsorbed on the catalyst.[19] The very slight decrease in activity (increase in T_{50}) indicates that the adsorbed water has little enhancement effect and that the sintering does not occur rapidly at 423 K.

Continued treatment of the catalysts at 423 K by hydrogen (IIb) and then by O_2 (IIc) also shows only slight effects upon the activity of all catalysts. Pretreatment IIb completely reduces the Au to Au^0 and no subsequent treatments (i.e., IIc, IId, or IIe) cause any change in the Au oxidation state, as determined by XANES. Since the Au is fully reduced, all observed CO oxidation is catalytic. Also, since the state obtained in IIb has the lowest T_{50} value for most catalysts, Au^0 is associated with the activity in these catalysts. The fact that all catalysts have comparable conversions (i.e., most show 50% conversion between 235 and 250 K) suggests that the crystallographic nature of the titania and the variable morphology that characterize the different polymorphs are not critical factors in determining the catalyst activity. All sintering by treatments after IIb must be related to migration of Au metal on the titanium oxide. For most catalysts, the reduction in H_2 slightly activates the catalyst, while subsequent treatment in oxygen (IIc) slightly deactivates it (Table 2). This reversal also refutes the possibility of progressive sintering and may suggest instead that H_2 has the effect of redispersing Au metal nanoparticles.

The effects of heating to 573 K in oxygen (IId) were mixed; in some catalysts, T_{50} increased, but in others, it was unchanged or even decreased. This implies that deactivation by either loss of water or sintering depends on other factors other than just the temperature of the treatment. One factor is the nature of the support. The higher loaded rutile-supported catalyst dramatically decreased in activity and did not recover as a result of subsequent reduction at lower temperature (IIe). This trend is apparent in Figure 11 and distinguishes it from the anatase and brookite. This deactivation and the remarkably lower overall activity for the lower loaded rutile sample suggest that certain properties of this support (crystal structure, defect structure, or the Au−titania interface contact) make it less effective as a support for the Au. The P25 is the next most affected by the 573 K calcination treatment, consistent with its significant concentration of the rutile phase. Brookite is one of the least affected by treatments.

The treatment in O_2 at 773 K decreased the activity of all catalysts (Table 2 and Supporting Information Figure s5). After the treatment, the reference WGC catalyst gave the highest activity of all catalysts and reached 50% conversion at 283 K. Consistent with lower temperature results, brookite-supported catalyst is still very active with a T_{50} value of 303 K. However, anatase- and P25-supported catalysts reached their 50% conversion at 373 and 400 K, respectively.

Another factor affecting activity is variation in the Au loading and areal density, which may possibly affect changes in dispersion upon deposition or during heat treatment. A comparison of the three anatase samples for both pretreatments in which the sample is calcined to 573 K (IId and IIIa) shows that they have comparable T_{50} values, suggesting that the variation in loading does not significantly affect the conversion in this loading range. Therefore, the calcined catalysts with lower loading make more effective use of the available Au. A

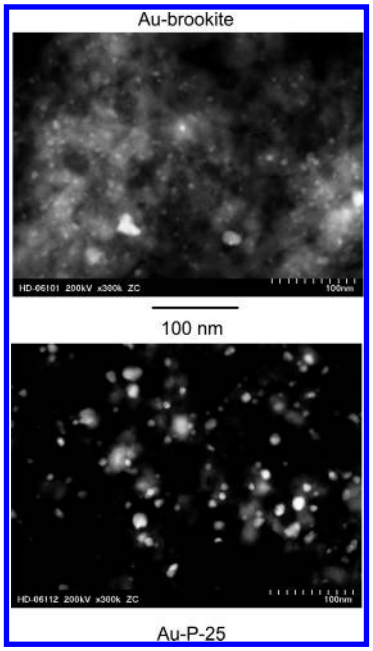

Figure 13. Au catalysts supported on brookite (3.3 wt % Au) and P25 (5.7 wt % Au) compared by conventional STEM after treatments up to 573 K (after sequence II).

comparison of the specific reaction rate (Table 3) shows that the effect of Au loading on the rate depends on the treatment. It has been noted previously by Moreau et al.[57] that the Au specific reaction rate frequently is observed to decrease with decreasing loading. They were able to achieve high specific activities at low loadings for catalysts without pretreatment (comparable to our as-synthesized state) and attributed this success to careful pH control during D−P in yielding uniform Au particle size distributions. The pH range (9−10) used by these authors corresponds to the range used in the present work. In our catalysts, we find comparable specific rates (within a factor of 2) for all loadings in the as-synthesized anatase, while calcination to 573 K seems to deactivate the catalyst with the highest loading. Interestingly, the reference WGC catalyst had the lowest loading and the highest specific activity of any we studied and it was presumably prepared using different synthesis (i.e., pH) conditions. The processes occurring during D−P have been described by Hermans and Geus,[58] and it is expected that the nucleation and size distribution of nascent Au particles depends on the solution concentration, pH, surface area, and surface structure of the oxide in complex ways. The effects of pH during D−P have been systematically measured by Zanella et al.[59] and Tsubota et al.[60]

Even more striking is the comparison between the rutile-supported catalyst and the anatase-supported catalyst. The rutile exhibits a strong dependence upon heat treatment and also upon Au loading. In particular, the rutile sample with a 2.9 wt % gold loading is very inactive at all stages compared with the anatase-supported catalyst with a 2.8 wt % gold loading which is active after all stages. The deactivation in the rutile samples during heat treatment is probably due to growth of large particle sizes, an assumption supported by the XRD in Figure 4 for the higher Au loading. The inactivity of the 2.9 wt % Au−rutile, even after reduction at 423 K, is also likely due to large particle size. The cause for such facile particle growth on rutile can only be conjectured but may be related to the density and/or configuration of surface vacancies and hydroxyls. These differences may be important either during D−P or during pretreatment.

It has been suggested that the high CO oxidation activity of Au−TiO_2 catalysts may be the result of the highly dispersed Au on the TiO_2 with the size in the range 2−3 nm.[12,16] The interaction between Au and TiO_2 plays an important role in stabilizing the Au particles. STEM results in Figures 3 and 6 reveal the presence of a large number of well-dispersed, small gold rafts (thin and 1−2 nm diameter) on the anatase and brookite supports for the as-synthesized catalysts. While the treatments in O_2 to 573 K (sequences II and III) caused considerable deactivation on rutile, it did not greatly affect the brookite-supported catalysts. It is of interest to further compare the microscopy results from these surfaces.

Figure 13 shows a comparison of the brookite-supported and P25-supported Au catalysts after completion of sequence II including calcination to 573 K. Z-contrast images recorded at identical magnification show clear differences in size distribution. Analysis of the particle sizes in these micrographs indicates that the mean particle size is 4.9 ± 3 and 8.2 ± 6 for the brookite and P25 supports, respectively. The smaller particles and narrower size distribution for the brookite-supported Au agrees with the absence of Au XRD features (Figure 5). The smaller Au mean particle size in the brookite is apparently correlated with its higher activity compared to the Au supported on P25 or the other supports.

The samples (Au−brookite) shown in Figure 6 were treated especially for purposes of performing microscopy. These three samples had comparable activities; that is, the conversion at 250 K was 28, 57, and 29% for the as-synthesized, reduced, and oxidized samples, respectively. Another Au−brookite sample was oxidized at 773 K for 1 h and exhibited a conversion of about 18% at 250 K. The activities confirm the relative insensitivity of the brookite-supported catalysts to high temperature processing indicated in Figure 11. A comparison of the micrographs in Figure 6 implies that the small "diffuse" raftlike particles observed on the as-synthesized and the mildly reduced samples are highly active. The micrograph of the samples treated at 573 K (Figure 6c), and others taken of this sample at comparable magnification, demonstrates the absence of these small diffuse rafts. They do show large numbers of faceted particles near 2−5 nm as well as a broad distribution of Au particles in the size range up to 70 nm, some fraction of which are also highly active for CO oxidation. Apparently, the activity of the brookite-supported Au is little affected by this striking change in particle morphology from raftlike to small faceted 3-D particles, but broadening of the size distribution to that observed on the P25 (Figure 13) does diminish activity. These results suggest that there is not a pronounced falloff in activity for particles smaller than 3 nm as has been previously suggested.[15]

Table 1 shows that the amount of Au adsorbed during D−P varies by a factor of 4 between catalysts with equal synthesis loadings. The total Au loading might be expected to depend on the surface area of the titania support. This variability is accounted for in the last column of Table 1 by dividing the Au loadings by the surface area of the support to obtain the areal density of the Au. The areal density also varies (by a factor of about 5) between different supports for comparable synthesis loading. In terms of either the total loading or the areal density, rutile takes on the highest amount of Au while brookite takes on the least for a 13% synthesis loading. Essential parameters (temperature, maturation time, pH, and washing) of the D−P conditions were held constant as closely as possible. Apparently,

the loading obtained is either dependent upon structural aspects of the TiO_2 support or extremely sensitive to details of the D−P conditions.

5. Summary and Conclusions

Titania-supported gold catalysts have been prepared by a standard deposition−precipitation process onto the surface of synthesized anatase, brookite, rutile, and commercial titania (P25). XRD demonstrates the structural purity of the titania phases in the supports. The structure and catalytic CO oxidation activity of the resulting catalysts have been determined after various pretreatments. Au is highly dispersed and cationic without pretreatment, but reaction conditions lead to Au reduction on-stream. Mild reduction at 423 K stabilizes the Au catalysts into raftlike clusters, and all Au catalysts are fully reduced and highly active after this treatment. This result suggests that activity of the raftlike Au is independent of the underlying titania structure. Treatments up to 573 K bring about deactivation, the extent of which depends on the titania support. Au supported on brookite is largely unaffected by treatment at this temperature, while rutile is more strongly affected. All catalysts show sintering of Au rafts into 3-D particles, but smaller sized 3-D particles remain active.

Acknowledgment. This research was sponsored by the Division of Chemical Sciences, Geosciences, and Biosciences, Office of Basic Energy Sciences, U.S. Department of Energy, under contract DE-AC05-00OR22725 with Oak Ridge National Laboratory, managed and operated by UT-Battelle, LLC. W.Y. and B.C. acknowledge the Oak Ridge National Laboratory Postdoctoral Research Associates Program administered jointly by the Oak Ridge Institute for Science and Education and Oak Ridge National Laboratory.

Supporting Information Available: Figures showing N_2 adsorption isotherms of sonicated anatase, sonicated rutile, hydrothermally synthesized Brookite, and commerical P25 and light-off curves of the catalysts. This material is available free of charge via the Internet at http://pubs.acs.org.

References and Notes

(1) Bond, G. C.; Sermon, P. A.; Webb, G.; Buchanan, D. A.; Wells, P. B. *J. Chem. Soc., Chem. Commun.* **1973**, 444.
(2) McIntosh, D.; Ozin, G. A. *Inorg. Chem.* **1976**, *15*, 2869.
(3) McIntosh, D.; Ozin, G. A. *Inorg. Chem.* **1977**, *16*, 51.
(4) Cha, D. Y.; Parravan, G. *J. Catal.* **1970**, *18*, 200.
(5) Galvagno, S.; Parravano, G. *J. Catal.* **1978**, *55*, 178.
(6) Haruta, M.; Yamada, N.; Kobayashi, T.; Iijima, S. *J. Catal.* **1989**, *115*, 301.
(7) Haruta, M.; Tsubota, S.; Kobayashi, T.; Kageyama, H.; Genet, M. J.; Delmon, B. *J. Catal.* **1993**, *144*, 175.
(8) Lin, S. D.; Bollinger, M.; Vannice, M. A. *Catal. Lett.* **1993**, *17*, 245.
(9) Yuan, Y. Z.; Asakura, K.; Wan, H. L.; Tsai, K. R.; Iwasawa, Y. *Chem. Lett.* **1996**, 755.
(10) Yuan, Y. Z.; Kozlova, A. P.; Asakura, K.; Wan, H. L.; Tsai, K.; Iwasawa, Y. *J. Catal.* **1997**, *170*, 191.
(11) Grunwaldt, J. D.; Kiener, C.; Wogerbauer, C.; Baiker, A. *J. Catal.* **1999**, *181*, 223.
(12) Bamwenda, G. R.; Tsubota, S.; Nakamura, T.; Haruta, M. *Catal. Lett.* **1997**, *44*, 83.
(13) Okumura, M.; Tanaka, K.; Ueda, A.; Haruta, M. *Solid State Ionics* **1997**, *95*, 143.
(14) Dekkers, M. A. P.; Lippits, M. J.; Nieuwenhuys, B. E. *Catal. Lett.* **1998**, *56*, 195.
(15) Valden, M.; Lai, X.; Goodman, D. W. *Science* **1998**, *281*, 1647.
(16) Valden, M.; Pak, S.; Lai, X.; Goodman, D. W. *Catal. Lett.* **1998**, *56*, 7.
(17) Grunwaldt, J. D.; Baiker, A. *J. Phys. Chem. B* **1999**, *103*, 1002.
(18) Mul, G.; Zwijnenburg, A.; van der Linden, B.; Makkee, M.; Moulijn, J. A. *J. Catal.* **2001**, *201*, 128.
(19) Date, M.; Ichihashi, Y.; Yamashita, T.; Chiorino, A.; Boccuzzi, F.; Haruta, A. *Catal. Today* **2002**, *72*, 89.
(20) Boccuzzi, F.; Chiorino, A.; Manzoli, M.; Andreeva, D.; Tabakova, T. *J. Catal.* **1999**, *188*, 176.
(21) Overbury, S. H.; Ortiz-Soto, L.; Zhu, H. G.; Lee, B.; Amiridis, M. D.; Dai, S. *Catal. Lett.* **2004**, *95*, 99.
(22) Costello, C. K.; Kung, M. C.; Oh, H. S.; Wang, Y.; Kung, H. H. *Appl. Catal., A* **2002**, *232*, 159.
(23) Kung, H. H.; Kung, M. C.; Costello, C. K. *J. Catal.* **2003**, *216*, 425.
(24) Knell, A.; Barnickel, P.; Baiker, A.; Wokaun, A. *J. Catal.* **1992**, *137*, 306.
(25) Grunwaldt, J. D.; Maciejewski, M.; Becker, O. S.; Fabrizioli, P.; Baiker, A. *J. Catal.* **1999**, *186*, 458.
(26) Haruta, M.; Kobayashi, T.; Tsubota, S.; Nakamura, T. *Chem. Express* **1988**, *3*, 159.
(27) Tsubota, S.; Yamada, N.; Haruta, M.; Kobayashi, T.; Nakahara, Y. *Chem. Express* **1991**, *5*, 349.
(28) Bond, G. C.; Thompson, D. T. *Gold Bull.* **2000**, *33*, 41.
(29) Bond, G. C.; Thompson, D. T. *Catal. Rev.—Sci. Eng.* **1999**, *41*, 319.
(30) Wolf, A.; Schuth, F. *Appl. Catal., A* **2002**, *226*, 1.
(31) Haruta, M. *Catal. Today* **1997**, *36*, 153.
(32) Schimpf, S.; Lucas, M.; Mohr, C.; Rodemerck, U.; Bruckner, A.; Radnik, J.; Hofmeister, H.; Claus, P. *Catal. Today* **2002**, *72*, 63.
(33) Zwijnenburg, A.; Saleh, M.; Makkee, M.; Moulijn, J. A. *Catal. Today* **2002**, *72*, 59.
(34) Haruta, M. *Cattech* **2002**, *6*, 102.
(35) Choudhary, T. V.; Goodman, D. W. *Top. Catal.* **2002**, *21*, 25.
(36) Schmid, G.; Corain, B. *Eur. J. Inorg. Chem.* **2003**, 3081.
(37) Kolmakov, A.; Goodman, D. W. *Surf. Sci.* **2001**, *490*, L597.
(38) Rodriguez, J. A.; Liu, G.; Jirsak, T.; Hrbek, J.; Chang, Z. P.; Dvorak, J.; Maiti, A. *J. Am. Chem. Soc.* **2002**, *124*, 5242.
(39) Pietron, J. J.; Stroud, R. M.; Rolison, D. R. *Nano Lett.* **2002**, *2*, 545.
(40) Yan, W. F.; Chen, B.; Mahurin, S. M.; Dai, S.; Overbury, S. H. *Chem. Commun.* **2004**, 1918.
(41) Riegel, G.; Bolton, J. R. *J. Phys. Chem.* **1995**, *99*, 4215.
(42) Borgarello, E.; Kiwi, J.; Pelizzetti, E.; Visca, M.; Gratzel, M. *J. Am. Chem. Soc.* **1981**, *103*, 6324.
(43) Hurum, D. C.; Agrios, A. G.; Gray, K. A.; Rajh, T.; Thurnauer, M. C. *J. Phys. Chem. B* **2003**, *107*, 4545.
(44) Mo, S. D.; Ching, W. Y. *Phys. Rev. B* **1995**, *51*, 13023.
(45) Maruska, H. P.; Ghosh, A. K. *Sol. Energy* **1978**, *20*, 443.
(46) Haruta, M.; Uphade, B. S.; Tsubota, S.; Miyamoto, A. *Res. Chem. Intermed.* **1998**, *24*, 329.
(47) Fukushima, K.; Takaoka, G. H.; Matsuo, J.; Yamada, I. *Jpn. J. Appl. Phys., Part 1* **1997**, *36*, 813.
(48) Iizuka, Y.; Tode, T.; Takao, T.; Yatsu, K.; Takeuchi, T.; Tsubota, S.; Haruta, M. *J. Catal.* **1999**, *187*, 50.
(49) Samonsov, G. V. *The Oxide Handbook*; IFI/Plenum: New York, 1982.
(50) Mizoguchi, T.; Tanaka, I.; Yoshioka, S.; Kunisu, M.; Yamamoto, T.; Ching, W. Y. *Phys. Rev. B* **2004**, *70*.
(51) Diebold, U. *Surf. Sci. Rep.* **2003**, *48*, 53.
(52) Huang, W. P.; Tang, X. H.; Wang, Y. Q.; Koltypin, Y.; Gedanken, A. *Chem. Commun.* **2000**, 1415.
(53) Zheng, Y. Q.; Erwei, S.; Cui, S. X.; Li, W. J.; Hu, X. F. *J. Mater. Sci. Lett.* **2000**, *19*, 1445.
(54) Lee, S.-J.; Gavrilidis, A. *J. Catal.* **2002**, *206*, 305.
(55) Schwartz, V.; Mullins, D. R.; Yan, W. F.; Chen, B.; Dai, S.; Overbury, S. H. *J. Phys. Chem. B* **2004**, *108*, 15782.
(56) Berndt, H.; Pitsch, I.; Evert, S.; Struve, K.; Pohl, M. M.; Radnik, J.; Martin, A. *Appl. Catal., A* **2003**, *244*, 169.
(57) Moreau, F.; Bond, G. C.; Taylor, A. O. *Chem. Commun.* **2004**, 1642.
(58) Hermans, L. A. M.; Geus, J. W. *Stud. Surf. Sci. Catal.* **1979**, *4*, 113.
(59) Zanella, R.; Giorgio, S.; Henry, C. R.; Louis, C. *J. Phys. Chem. B* **2002**, *106*, 7634.
(60) Tsubota, S.; Cunningham, D. A. H.; Bando, Y.; Haruta, M. Studies in Surface Science and Catalysis. In *Preparation of Catalysts VI: Scientific Bases for the Preparation of Heterogeneous Catalysts*; Poncelet, G., Ed.; Elsevier: Amsterdam, The Netherlands, 1995; Vol. 91, p 227.